$B\rho$-DEPENDENT TAYLOR TRANSFER MAPS FOR THE SUPER-FRS DIPOLE MAGNETS

E. Kazantseva, O. Boine-Frankenheim, TEMF TU-Darmstadt, Darmstadt, Germany
H. Weick, J. S. Winfield, GSI Helmholtzzentrum für Schwerionenforschung, Darmstadt, Germany
M. Berz, R. Jagasia, K. Makino, Michigan State University, East Lansing, USA

Abstract

We discuss the iron saturation effects in large aperture separator magnets. A method is introduced that allows the calculation of accurate Taylor transfer maps for iron-dominated magnetic elements and an arbitrary magnetic rigidity $B\rho$. The method is applied to the Super-FRS preseparator 11° dipole magnet revealing a significant $B\rho$-dependency of some transfer map elements. The convergence of the transfer maps in terms of their order and the number of magnetic field expansion points along the reference path is discussed.

INTRODUCTION

The Super-FRS (SFRS) is an in-flight projectile fragment separator being built at GSI for FAIR [1, 2]. Due to the required high design momentum resolution as well as the large geometric and momentum acceptance (A_h= ±40 mrad, A_v = ±20 mrad, $\Delta p/p$= ±2.5 %) the dipole magnets of the SFRS have large apertures of $120 \times 14\,\mathrm{cm}^2$ for the preseparator and $38 \times 14\,\mathrm{cm}^2$ for the main separator dipole magnets. The wide design particle magnetic rigidity $B\rho$ range of 2-20 Tm requires the variation of the main dipole magnetic field B_0 in the range of 0.15-1.6 T and of the coil current I from 60 A to 643 A. Since the magnetic field in the pole gap depends on its distribution in the yoke, a high and constant relative magnetic permeability μ_r of the yoke material is desired. However, in reality μ_r is a non-linear function of the magnetic field strength $H(I)$ and approaches unity for high H values (B-H saturation). Moreover, geometrical non-uniformities of the yoke like edges or holes affect H and B locally, which leads to I-dependent local μ_r changes. These effects propagate in the field distribution in the pole gap and influence the nonlinear particle dynamics.

For the particle separators and spectrometers like Super-FRS it is important to have a highly accurate fast computational ion-optical model with good predictability, especially if rare particles with low production rates in high $B\rho$ range are studied. Thus, it is crucial to take possible saturation effects into account. Therefore, we have developed an approach allowing to derive the $B\rho$-dependent transfer maps.

We calculated transfer maps for the radiation resistant, normal conducting dipole magnet of the SFRS preseparator with a deflection angle $\theta_0 = 11°$ and radius $R_0 = 12.5$ m [3]. It can be expected that the $B\rho$ dependence is similar for all SFRS dipole magnets, because they will be operated with the same B_0 range. Our ion-optical model is based on Taylor transfer maps [4] computed with COSY INFINITY [5]. The transfer maps were obtained by a numerical integration of ODEs of motion using a simulated field distribution and the differential algebraic (DA) Runge-Kutta method of the 8th order [4, 6].

For the magnetic field simulations a magnetization curve B-H was measured for the prototype of the considered magnet by means of the method described in [7]. In Fig. 1 **a)** and **b)** the B-H and the μ_r-B curves are shown, respectively.

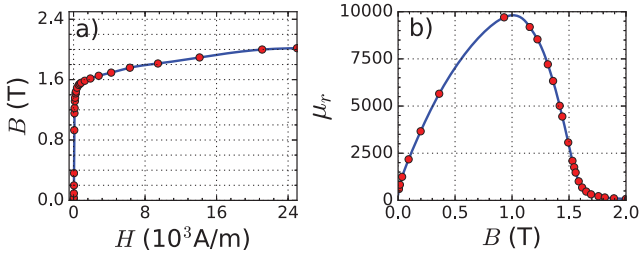

Figure 1: Measured magnetization curve (red dots) plotted together with its spline interpolation (blue line) as **a)** B versus H and **b)** μ_r versus B.

MAGNETIC FIELD CALCULATION

The magnetic field was simulated for different excitation currents using the finite element method (FEM) in CST EMS [8] and the surface integration Helmholtz method (SIHM) [9, 10] in COSY INFINITY.

In the SIHM, the Helmholtz vector field decomposition theorem for a finite volume $\vec{B}(\vec{r}) = \vec{\nabla} \cdot \varphi(\vec{r}) + \vec{\nabla} \times \vec{A}(\vec{r})$ is used, where φ and $\vec{A}$ are the scalar and the vector potential, respectively. Utilizing the fact that the magnetic field satisfies the Laplace equation, the scalar and vector potentials inside the volume of interest Ω (surrounded by the surface $\partial\Omega$ with given magnetic field data) are calculated by

$$\varphi(\vec{r}) = \frac{1}{4\pi} \int_{\partial\Omega} \frac{\vec{n}(\vec{r}_s) \cdot \vec{B}(\vec{r}_s)}{|\vec{r} - \vec{r}_s|} ds, \quad (1)$$

$$\vec{A}(\vec{r}) = -\frac{1}{4\pi} \int_{\partial\Omega} \frac{\vec{n}(\vec{r}_s) \times \vec{B}(\vec{r}_s)}{|\vec{r} - \vec{r}_s|} ds. \quad (2)$$

Here $\vec{r}_s$ is a vector of the position on $\partial\Omega$, $\vec{r} = (X, Y, Z)$ is a vector of the position inside Ω and $\vec{n}(\vec{r}_s)$ is a normal to the surface. The integrands in Eq. (1) and (2) are expanded in Taylor series in both surface and volume variables. The integration is performed using the DA antiderivation operation [4] resulting in a DA vector $\vec{B}(X, Y, Z)$.

For the SFRS dipole magnet we used the magnetic field vector values on the surface of a box $D = \{X \in [-0.6, 0.6]$ m, $Y \in [-0.07, 0.07]$ m, $Z \in [-2.2, 2.2]$ m$\}$ to determine $\vec{B}(X, Y, Z)$ along the horizontally laid reference

ISBN 978-3-95450-182-3

path. Both the reference path and the right handed coordinate system with the origin in the center of the magnet are shown in Fig. 2 **a)**. The vertical coordinate Y is normal to the paper plane. The variable S is the path length along the reference trajectory starting well outside of the dipole where $|\vec{B}|$ is negligibly small. The entire path of the reference trajectory is placed inside the box D. The field $\vec{B}(\vec{r}_s)$ on the surface of D was obtained using FEM and interpolated with quadratic polynomials via the least square method.

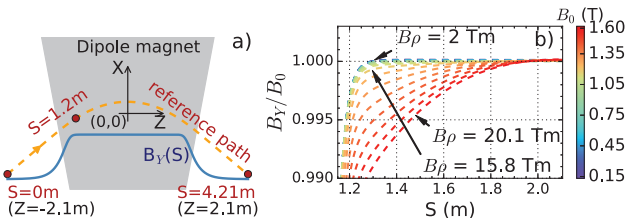

Figure 2: **a)** Schematic of the dipole magnet coordinate system with reference path and magnetic field $B(S)$, where S is the position along the reference path. **b)** Normalized magnetic field $B(S)/B_0$ calculated for different B_0 values.

In order to generate the transfer map for an arbitrary $B\rho$ by DA integration, it is necessary to know the I dependence of $\vec{B}$. Since 3D simulations or measurements of the magnetic field are expensive, they can only be performed for a finite number of I values. Therefore, we simulated $\vec{B}$ for 25 equidistantly spaced I values covering the required $B\rho$ range. Between the simulated points we interpolated each component of $\vec{B} = (B_X, B_Y, B_Z)$ piecewise by 3rd order polynomials

$$B_\alpha(I) \approx b_0^\alpha + b_1^\alpha(I - I_0) + b_2^\alpha(I - I_0)^2 + b_3^\alpha(I - I_0)^3, \quad (3)$$

where $\alpha \in \{X, Y, Z\}$, $b^\alpha_{0,1,2,3}$ are fit parameters and I_0 is middle point of the chosen current interval. Using the fact that the magnetic field in the gap of a dipole is a solution of the Laplace equation together with the linearity of the Laplace operator, we can apply the SIHM to the coefficients $b^\alpha_{0,1,2,3}$ to get their DA values along the reference path.Then the DA vector $\vec{B}(X, Y, Z, I - I_0)$ can be obtained easily using Eq. (3), where now $(I - I_0)$ is an additional DA variable.

CURRENT DEPENDENCE OF MAGNETIC FIELD AND REFERENCE TRAJECTORY

A well known consequence of the B-H saturation in iron is the effective shortening of dipole magnets. This is caused by the drastic local decrease of μ_r at the edges of the poles for high B_0 values. The effect is illustrated in Fig. 2**b)** where relative magnetic field between the entrance and the center of the magnet is depicted revealing a significant drop of B of ~ 1 % at the edge for $B\rho > 16$ Tm ($B_0 > 1.3$ T).

The effective length (or length of the equivalent hard-edge model) of a dipole magnet normally defined as

$$L^0_{eff} = \frac{\int_{-\infty}^{\infty} B(S)dS}{B_0} \quad (4)$$

decreases with increasing $B\rho$. In case of the SFRS dipole L^0_{eff} drops from 2401 mm at $B\rho = 2$ Tm to 2389 mm at $B\rho = 20$ Tm as shown in Fig. 3 **a)**. For a standalone magnet this L^0_{eff} difference of 12 mm would lead to an under- or over-deflection of the reference particle of up to 0.5 mrad. In SFRS, the dipole magnets do not stand alone, but are grouped in triples. The grouping allows to correct the deflection angles of the whole triple by empirical tuning of B_0 for each dipole and each $B\rho$ value. The solution of this problem is not unique as well as the resulting reference trajectory, which changes the non-linear particle dynamics. Furthermore, the optimization procedure is time-consuming and has to be performed during beam time.

Alternatively, one optimal solution with invariant reference path outside the magnet can be found in advance by forcing the effective length to equal $\theta_0 R_0$ for each dipole and $B\rho$. This can be achieved by using $B_{eff} = B\rho/R_0$ instead of B_0 in Eq. (4). Then the effective length can be written as

$$L_{eff} = \frac{\int_{-\infty}^{\infty} B(S)dS}{B_{eff}} = \int_{-\infty}^{\infty} \frac{B(S)}{B\rho} dS \cdot R_0 = \theta R_0, \quad (5)$$

where θ is the actual deflection angle. In order to achieve $\theta(B\rho) = \theta_0 = \text{const.}$ ($\Leftrightarrow L_{eff}(B\rho) = \text{const.}$), the problem $v_X(I)|_{Z=0} = 0$ should solved numerically for each $B\rho$, where v_X is the horizontal transversal velocity of the reference particle. The resulting coil current I_{opt} defines the optimal B. For the SFRS dipole magnet a constant $L_{eff}(B\rho)$ value of 2.4 m was obtained as shown in Fig. 3 **a)**. The corresponding reference trajectories for different $B\rho$ values reveal only slight transversal deviations of ± 0.1 mm in the middle of the magnet as shown in Fig. 3 **b)**. These lead to small variations of the pathlengths below 10 μm, which often can be neglected. The trajectories are identical in the start and the end points ($Z = \pm 2.1$ m) due to the symmetry of the magnetic field around the XY-plane. However, for a non-symmetric magnetic field, the reference paths will have slightly varying X-positions for different $B\rho$ values at the exit. In this case the total effective length of all three magnets should be forced to be constant. Still it can be expected that the resulting transfer maps of single dipoles will not change drastically. Therefore, the stand-alone dipole can be used to study the $B\rho$ dependences of the transfer maps.

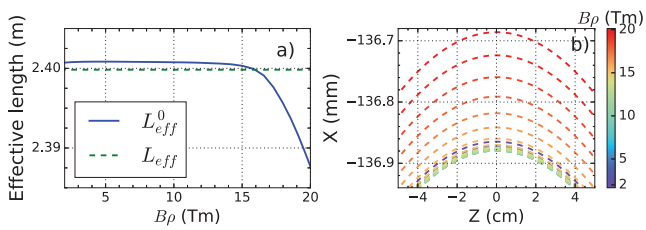

Figure 3: **a)** Calculated effective lengths L^0_{eff} and L_{eff} as function of $B\rho$ and **b)** optimal reference path for different Bρ values at the center of the magnet.

$B\rho$-DEPENDENT TRANSFER MAPS

The transfer maps were generated for the $B\rho$ range of 2-20 Tm by means of numerical integration of the ODEs of motion using $\vec{B} = \vec{B}(X, Y, Z, I - I_0)$. In Fig. 4 selected transfer map elements in TRANSPORT notation [11] are plotted as functions of $B\rho$. A significant $B\rho$ dependence can be observed already for the 1st order elements $(a|x)$ and $(b|y)$, which vary about ±0.9 % and ±5.5 %, respectively. Alternatively, these elements can be calculated by

$$(a|x) = \frac{\partial}{\partial x}\int_0^{S_{max}} \frac{v_Y(S)B_Z(S) - v_Z(S)B_Y(S)}{B\rho} dS, \quad (6)$$

$$(b|y) = \frac{\partial}{\partial y}\int_0^{S_{max}} \frac{v_Z(S)B_X(S) - v_X(S)B_Z(S)}{B\rho} dS, \quad (7)$$

where S_{max} is the path length, v_Z and v_X were deduced geometrically, and the $B\rho$ dependence of the reference trajectory is neglected. The "Map" and "Integral" curves in Fig. 4 obtained from the transfer maps and Eq. (6,7), respectively, are in good agreement proving that the $B\rho$ dependency originates from the B-H saturation in the yoke. The form of the elements $(a|x)$ and $(b|y)$, which is defined by relative $\vec{B}$ changes (see Eq. 6 and 7), shows that the $B\rho$ dependence plays a role already for small B_0 values. However, the other 1st order elements have only a small $B\rho$ dependence below ±0.1 % as shown for $(l|\delta)$ exemplarily. For the 2nd order elements the variation with $B\rho$ can be much higher like for $(a|xx)$, which falls by 75 % in the considered $B\rho$ range.

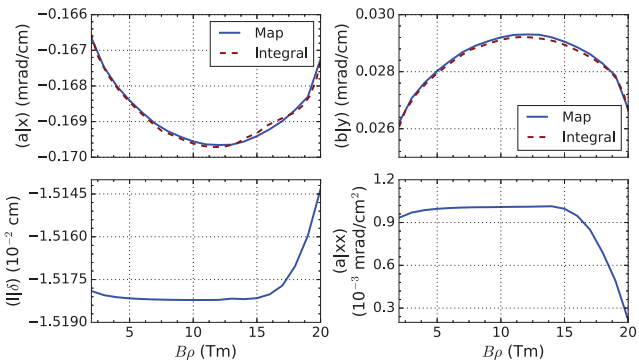

Figure 4: Transfer map elements of the of 1st and 2nd order versus $B\rho$ calculated for the SFRS dipole magnet.

TRANSFER MAP'S CONVERGENCE

To measure the convergence of the transfer map $\boldsymbol{M}$, we used the weighted relative norm $N_W(w) = \langle \boldsymbol{M}(\boldsymbol{W} \cdot \vec{d}_{max})/(\boldsymbol{W} \cdot \vec{d}_{max})\rangle$, where $\vec{d}_{max}$ is the largest allowed deviation of a particle with respect to the reference trajectory in 6D phase space, $w \in (0, 1]$ is a weight factor and $\boldsymbol{W}$ is a diagonal matrix with entries $w_{ii} = \pm w \; \forall \; i = 1,...,6$. Thus, the vectors $\boldsymbol{W} \cdot \vec{d}_{max}$ are positions at the scaled border of the phase space.

Assuming that the deviated particles are equidistributed within the SFRS acceptance, we can define the vector standard deviation $\xi \vec{d}_{max}$ in the phase space, where $\xi = 1/\sqrt{3}$. As shown in Fig. 5 **a)** the transfer map of the SFRS dipole converges fast with increasing of the order for $w \leq 0.75\xi$, but diverges for $w \geq \xi$. The reason for this norm behavior is the Taylor expansion nature of the used magnetic field which becomes less accurate with the increasing distance to the points of expansion (PoE).

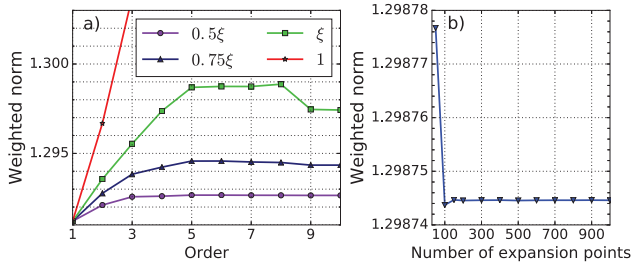

Figure 5: Calculated weighted map norms N_W as function of **a)** the order for different weights w and **b)** the number of the expansion points along the reference path at $w = 0.5\xi$ and the 7th order.

The long computation times for the higher orders of SIHM make it impractical to use it online for the transfer map calculation. Thus, the field has to be precalculated in a set of PoE along the reference path. Between the points the field can be estimated from the Taylor polynomial corresponding to the nearest PoE. The closer the points are, the higher is the accuracy of the estimation. Figure 5 **b)** shows N_W for the 7th order in dependence on the number of equidistantly distributed PoE. Accordingly, the transfer map convergates already at about 150 (distance 2.8 cm).

CONCLUSION

A universal approach to generate accurate $B\rho$-dependent transfer maps for iron-dominated ion-optical elements has been developed and applied to the SFRS dipole magnet. The resulting transfer maps revealed a distinct Bρ dependency. Investigations of the transfer map norm showed a rapid convergence with rising order for weigths of up to 0.5ξ as well as with increasing density of expansion points.

ACKNOWLEDGEMENT

E.K. thanks F. Klos and H. Leibrock for the support on the magnetic field measurements and calculations. This work is financially supported by GSI. The hardware to perform parallel computations and development of algorithms are financially supported by the U.S. Department of Energy.

REFERENCES

[1] H. Geissel *et al.*, "The Super-FRS project at GSI", *Nucl. Instr. Meth.*, vol. B204, pp. 71–85, 2003.

[2] H. Geissel and M. Winkler for the Super-FRS collaboration, "Technical design report of the Super-FRS", GSI, Darmstadt, Germany, Dec. 2008.

[3] C. Muehle *et al.*, "Radiation resistant prototype dipole for the first stage of Super-FRS", *IEEE Trans. Appl. Supercond. vol. 22, issue 3, p. 4003304, June 2012.*

[4] M. Berz, *Modern map methods in particle beam physics*, San Diego, CA, USA: Acad. Press 1999.

ISBN 978-3-95450-182-3

[5] K. Makino and M. Berz, "COSY INFINITY Version 9", *Nucl. Instr. Meth.*, vol. A558, pp. 346–350, 2006.

[6] K. Makino, "The COSY 8th order Runge-Kutta integrator", *MUC-NOTE-COOL_THEORY-238*, Neutrino Factory/Muon Collider Notes, March 2002.

[7] K. N. Henrichsen, "Permeameter", in *Proc. The Conf. On Magn. Technol.*, Chilton, UK, July 1967, pp. 735–739.

[8] CST EMS, `https://www.cst.com/products/cstems`

[9] S. Manikonda, M. Berz, "Multipole expansion solution of the Laplace equation using surface data", *Nucl. Instr. Meth.*, vol. A558, pp. 175–183, 2006.

[10] S. Manikonda, "High order finite element methods to compute Taylor transfer maps", Ph.D. thesis, Dept. of Phys. and Astron., Michigan State University, East Lansing, USA, 2006.

[11] K. L. Brown, "The Ion Optical Program TRANSPORT", SLAC, Menlo Park, USA, Techn. Rep. No. 91, 1979.